

The Lynden-Bell bar formation mechanism in simple and realistic galactic models

E. V. Polyachenko,^{1*} I. G. Shukhman,^{2†}

¹*Institute of Astronomy, Russian Academy of Sciences, 48 Pyatnitskaya St., Moscow 119017, Russia*

²*Institute of Solar-Terrestrial Physics, Russian Academy of Sciences, Siberian Branch, P.O. Box 291, Irkutsk 664033, Russia*

21 August 2020

ABSTRACT

Using the canonical Hamilton-Jacobi approach we study the Lynden-Bell concept of bar formation based on the idea of orbital trapping parallel to the long or short axes of the oval potential distortion. The concept considered a single parameter – a sign of the derivative of the precession rate over angular momentum, determining the orientation of the trapped orbits. We derived a perturbation Hamiltonian which includes two more parameters characterising the background disc and the perturbation, that are just as important as the earlier known one. This allows us to link the concept with the matrix approach in linear perturbation theory, the theory of weak bars, and explain some features of the nonlinear secular evolution observed in N-body simulations.

Key words: Keywords: galaxies: bar, galaxies: kinematics and dynamics

1 INTRODUCTION

A remarkable paper by Lynden-Bell (1979) had influenced the bar formation theory in stellar discs and the radial-orbit instability theory in spherical clusters (e.g. Polyachenko & Shukhman 2015). It considers a weak oval distortion of the potential (bar) rotating with pattern speed Ω_p . A substantial group of stars within the corotation radius obey a condition

$$|\Omega - \Omega_p - \frac{1}{2}\varkappa| \ll \Omega \quad (1.1)$$

to which we will refer below as ‘the slowness condition’. Here Ω and \varkappa denote the angular speed and the epicyclic frequency of radial oscillations. In the reference frame of the bar, the motion of these stars can be viewed as slow nodal precession of stellar orbits, as long as the fast motion of stars along the orbits can be averaged out.

Lynden-Bell suggested a very elegant qualitative way to describe the dynamics of these orbits, in particular, their ability to align parallel to the long/short axis of the potential thereby reinforcing/weakening the primordial oval perturbation. Recall that orbits in such a weakly non-axisymmetric system possess a specific integral of motion $J_f = L/2 + I$, while the angular momentum L and radial action I of the star is changing. The key insight was that if the precession rate decreases/grows with L (at constant J_f), such orbits seek for stationary position perpendicular/parallel

to the bar. The former orbits were declared as ‘normal’, whereas the latter declared ‘abnormal’ since they occupy only a small fraction of the phase space in the centre of the disc. Mathematically, the ‘normal’/‘abnormal’ orbits have negative/positive derivative of the precession rate over L at constant J_f . Given the importance of this derivative in stellar dynamics (of the precession rate, distribution functions, etc.), we began to call it ‘LB-derivative’ (Polyachenko 2004, 2005).

Matrix methods of linear perturbation theory for study instability in the disc and spherical stellar systems show that sign of the precession rate is an important parameter. For instance, the loss cone instability (Polyachenko 1991; Tremaine 2005; Polyachenko et al. 2007, 2008) is sensitive to the sign of the precession rate itself, not to the sign of its derivative. On the other hand, Merritt (1985), and then Saha (1991); Weinberg (1991); Palmer (1994) used the Lynden-Bell idea to explain a mechanism of the radial-orbit instability (ROI) in spherical systems. This idea indeed can be justified in the case of extremely slow ROI, although generally, it is invalid (see details in Polyachenko & Shukhman 2015). This hints to the existence of other parameters in addition to the LB-derivative of the precession rate governing the orbital alignment.

It is also worth noting that the theory of weak bars suggests orbits’ alignment parallel to the long axis of the potential from the corotation resonance (CR) inside up to the centre or the inner Lindblad resonance (ILR) (Sanders & Huntley 1976; Binney & Tremaine 2008, hereafter BT). In contrast, the Lynden-bell mechanism (within

* E-mail: epolyach@inasan.ru

† E-mail: shukhman@iszf.irk.ru

the region of applicability inside CR) predicts the orbital alignment parallel to the short axis of the potential everywhere excluding a small central region where the LB-derivative is positive.

The goal of this paper is to analyse the problem consistently using a standard rigorous technique of finding stationary points parenting families of trapped orbits. Section 2 describes the technique in a short form. Section 3 contains two analytic examples (the power-law angular speed and the isochrone potential) and results of N-body simulations of a realistic Milky Way model. Finally, in Section 4 we discuss and summarise the results.

2 THE HAMILTONIAN-JACOBI APPROACH FOR STATIONARY POINTS

In this section, we employ the standard formalism to find families of orbits trapped by the bar potential. To this end, we find stationary points of the Hamiltonian equations that mark closed elliptical orbits parenting families of trapped orbits. These closed orbits are analogues of circular orbits in axisymmetric potentials. The stellar motion is considered in the epicyclic approximation, and the bar pattern speed Ω_p obeys the slowness condition (1.1).

The Jacobi integral for axisymmetric potential $\Phi_0(r)$ in the rotating frame can be written as

$$H_0(L, I) = \frac{1}{2} \Omega^2(R) R^2 + \Phi_0(R) - \Omega_p L + \varkappa(R) I + \beta(R) I^2, \quad (2.1)$$

where $R = R(L)$ is the guiding centre radius. In order to obtain linear corrections $\propto \mathcal{O}(I)$ for the angular speed $\Omega(R)$ and the epicyclic frequency $\varkappa(R)$, we retain a small post-epicyclic term βI^2 . An explicit form of β can be found, e.g., in Shu (1969), Contopoulos (1975), Mark (1976) and Bertin (2014):

$$\beta = \frac{1}{8R^2} \left(3q - \frac{1}{3} q^2 + \frac{1}{2} R \frac{dq}{dR} \right), \quad q = \frac{d \ln(\varkappa^2)}{d \ln R}. \quad (2.2)$$

From (2.1) we obtain:

$$\Omega_1(L, I) \equiv \frac{\partial H_0(L, I)}{\partial I} = \varkappa + 2\beta I + \mathcal{O}(I^2), \quad (2.3)$$

$$\Omega_2(L, I) \equiv \frac{\partial H_0(L, I)}{\partial L} = \Omega - \Omega_p + \frac{d\varkappa}{dL} I + \mathcal{O}(I^2). \quad (2.4)$$

The orbit precession rate in the rotating frame is

$$\Omega_{\text{pr}}(L, I) \equiv \Omega_2(L, I) - \frac{1}{2} \Omega_1(L, I). \quad (2.5)$$

Let's $\delta\Phi$ be a weak oval distortion of the axisymmetric disc potential $\Phi_0(r)$ rotating with pattern speed Ω_p ,

$$\delta\Phi(r, \varphi) = A(r) \cos(2\varphi), \quad A < 0. \quad (2.6)$$

This form suggests that troughs of the potential and crests of the perturbed surface density are oriented along the horizontal axis OX . A full Hamiltonian H_J is then equal to a sum of the Jacobi integral (2.1) and the perturbed potential (2.6), $H_J = H_0 + \delta\Phi$.

Following Polyachenko (2004, 2005), we perform transformation of action-angle variables

$$I \rightarrow J_f = I + \frac{1}{2} L, \quad w_2 \rightarrow \phi = w_2 - \frac{1}{2} w_1 \quad (2.7)$$

to benefit from having slowly varying angle variable ϕ compared to w_1 , provided that Ω_p obeys (1.1). Averaging the Jacobi integral (2.1) over w_1 gives a new integral of motion J_f . Using the epicyclic approximation,

$$r = R - \rho \cos w_1, \quad \varphi = \phi + \frac{1}{2} w_1 + \frac{2\Omega}{\varkappa} \frac{\rho}{R} \sin w_1, \quad (2.8)$$

one can have for the averaged bar potential:

$$V(L, J_f, \phi) = \frac{1}{2\pi} \oint \delta\Phi(r(L, J_f, w_1), \varphi(L, J_f, w_1, \phi)) dw_1 = B(L, J_f) \cos(2\phi), \quad (2.9)$$

where $\rho = (2I/\varkappa)^{1/2}$ is the epicyclic radius,

$$B(L, J_f) = -\frac{A(R)}{2} \left(\frac{\rho}{R} \right) \left(\frac{R}{A} \frac{dA}{dR} + \frac{4\Omega}{\varkappa} \right). \quad (2.10)$$

From (2.7) and (2.8) we infer that orbit's apocentre is parallel to the long axis of the potential if angle variable $\phi = \frac{1}{2}\pi$ or $\frac{3}{2}\pi$, and to the short axis if $\phi = 0$ or π .

Omitting the terms depending on J_f only, one can end up with the following expression for the Hamiltonian averaged over the fast orbital motion:

$$\mathcal{H}_J(I, \phi) = -2\mathcal{Q}I + 2\mathcal{P}I^2 + V(L, J_f, \phi) = -2\mathcal{Q}I + 2\mathcal{P}I^2 + b(L) I^{1/2} \cos(2\phi). \quad (2.11)$$

The coefficients \mathcal{Q} and \mathcal{P} are the precession rate of the orbits in the rotating frame and the LB-derivative of the precession rate in the limit of small I :

$$\mathcal{Q} \equiv \Omega_{\text{pr}}(L, 0), \quad (2.12)$$

$$\mathcal{P} \equiv \frac{d\mathcal{Q}}{dL} - \frac{1}{2} \frac{d\varkappa}{dL} + \frac{1}{2} \beta. \quad (2.13)$$

If ILRs are present, \mathcal{Q} is positive between the first (inner) and the second (outer) ILRs. In the absence or outside ILRs, \mathcal{Q} is negative. Factor $bI^{1/2}$ in the last term of the Hamiltonian substitutes the amplitude of the averaged bar potential $B(L, J_f)$ (see 2.10). The new parameter

$$b(L) = -\frac{A(R)}{2} \left[\frac{2}{\varkappa R^2} \right]^{1/2} \left(\frac{R}{A} \frac{dA}{dR} + \frac{4\Omega}{\varkappa} \right) \quad (2.14)$$

reflects the orbital *responsiveness* to the bar-like perturbation.

Note that in fact \mathcal{Q} , \mathcal{P} , and b are functions of invariants, so no derivation over I is needed. Within the adopted approximation, however, these invariants can be replaced by L (or R). To justify this, one needs to consider a small perturbation of the angular momentum, $h \equiv L - L_0$, near the angular momentum L_0 of the circular orbit on a given radius. The scaling adopted in this paper is the following: $h, I, \mathcal{Q} = \mathcal{O}(\varepsilon^{2/3})$ and $\mathcal{P} = \mathcal{O}(1)$, where ε is a small parameter characterising the oval distortion, i.e. $A = \mathcal{O}(\varepsilon)$. In doing so, we obtain $\mathcal{Q} = \Omega_{\text{pr}}(J_f, 0)$ and $\mathcal{P} = \mathcal{P}(L_0)$. Changing J_f and L_0 in the arguments of these functions to L gives additional terms of the order $\mathcal{O}(\varepsilon^2)$ which are smaller than all terms retained in the Hamiltonian ($\mathcal{O}(\varepsilon^{4/3})$). The detailed derivation can be found in Polyachenko & Shukhman (2020).

Similar technique based on the averaged Jacobi Hamiltonian near ILR for spiral perturbations using the post-epicyclic approximation including the terms up to $(I^{1/2})^4$ was elaborated in Contopoulos (1975), but it differs in some

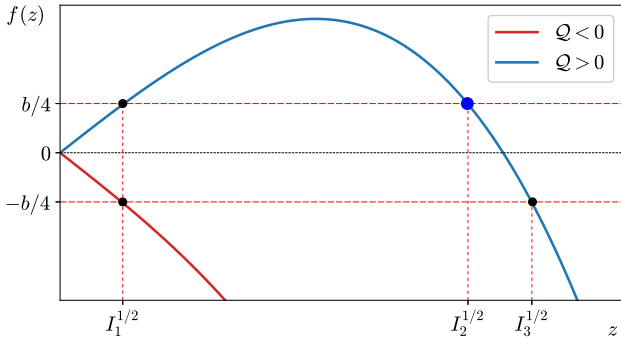


Figure 1. Solutions of eqs. (2.17, 2.18) for $\mathcal{P} > 0, b > 0$.

details. Apart from the different form of perturbation, there are distinctions in the derivation of the averaged Hamiltonian. In particular, Contopoulos considered L_0 as the angular momentum of stars exactly on ILR, while in our case, L_0 is the angular momentum of any orbit obeying (1.1); the ILR may be absent. Besides, two small parameters of the problem – the amplitude of the spiral potential A and the epicyclic parameter I ($\sim h$), were considered as independent ones, while in our case they are related by the scaling given above. The latter allows us to obtain the final results much easier.

Stationary points are derived from the equations:

$$\frac{\partial \mathcal{H}_J}{\partial \phi} = 0, \quad \frac{\partial \mathcal{H}_J}{\partial I} = 0, \quad (2.15)$$

which yield

$$\sin(2\phi) = 0, \quad \mathcal{Q} I^{1/2} - 2\mathcal{P} I^{3/2} - \frac{1}{4} b \cos(2\phi) = 0. \quad (2.16)$$

Finally, we obtain the next conditions for the radial actions:

$$f(I^{1/2}) = \frac{1}{4} b \quad (\text{short axis: } \phi = 0, \pi), \quad (2.17)$$

$$f(I^{1/2}) = -\frac{1}{4} b \quad (\text{long axis: } \phi = \pi/2, 3\pi/2), \quad (2.18)$$

where $f(z) = \mathcal{Q}z - 2\mathcal{P}z^3$.

The negative sign of b essentially occurs at the end of the bar, i.e. in the vicinity of the corotation, see discussion below. Thus we shall mainly assume $b > 0$; the opposite case will be treated separately.

To illustrate solutions of the last equations, we shall consider ‘abnormal’ orbits, $\mathcal{P} > 0$. In case of $\mathcal{Q} > 0$, function $f(z)$ have maximum $b_{\text{crit}}/4$ (see Fig. 1), where

$$b_{\text{crit}} \equiv \frac{8|\mathcal{Q}|}{3} \left(\frac{\mathcal{Q}}{6\mathcal{P}} \right)^{1/2}. \quad (2.19)$$

If $b < b_{\text{crit}}$, eq. (2.17) has two solutions, otherwise there is no solution. Similarly, no solutions of this equation exist for $\mathcal{Q} < 0$. One solution of eq. (2.18) corresponding to the closed orbit parallel to the long axis (L-orbit) exists for any signs of \mathcal{Q} and $(b - b_{\text{crit}})$. The latter is often called the sequence x_1 (e.g., BT, sect. 3.3.2). The former solutions correspond to the closed orbits oriented parallel to the short axis of the potential (S-orbit): one with the lower eccentricity is stable (sequence x_2), and another one is unstable (sequence x_3).

All phase portraits are given in Fig. 2. The described

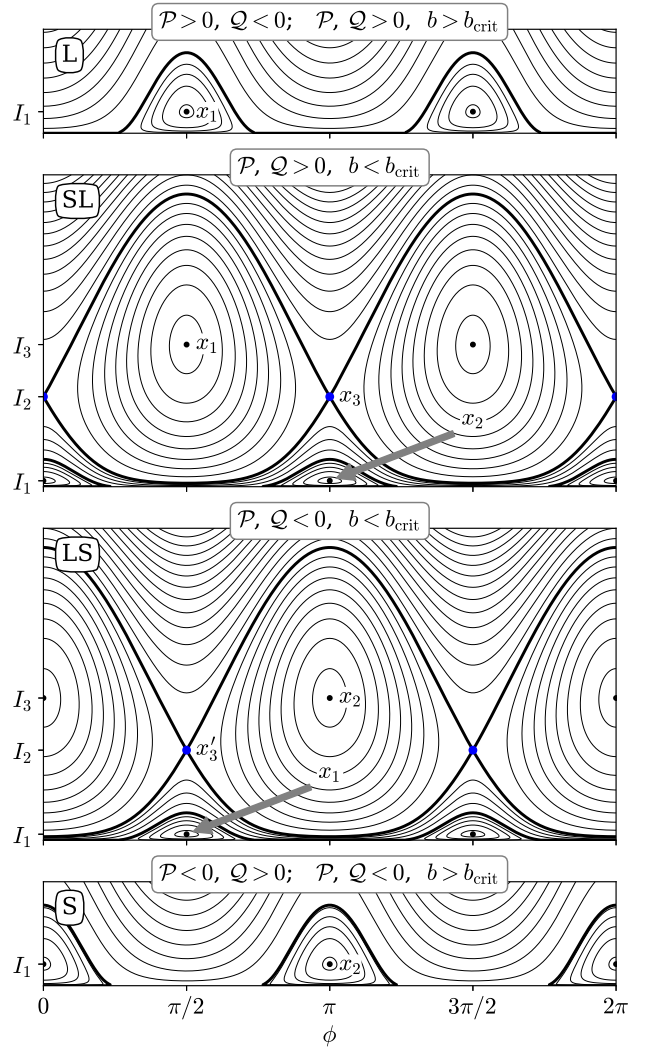


Figure 2. Phase portraits in $(\phi-I)$ planes of the averaged Hamiltonian (2.11) for $b > 0$. The closed L-orbits correspond to $\phi = \pi/2, 3\pi/2$ (sequence x_1), the closed S-orbits – to $\phi = 0, \pi, 2\pi$ (sequence x_2). The saddle points I_2 (blue dots) correspond to unstable sequences x_3 and x_3' .

above ‘abnormal’ orbits, $\mathcal{P} > 0$, give portraits (L) or (SL).¹ Outside ILRs, only sequence x_1 is possible. Between ILRs the sequence x_1 becomes more eccentric and a new sequence of S-orbits x_2 may appear, if the bar amplitude is sufficiently small ($b < b_{\text{crit}}$). The phase portraits for the ‘normal’ orbits, $\mathcal{P} < 0$, are shifted by $\pi/2$ for the opposite sign of \mathcal{Q} : sequence x_1 is turned into x_2 (panels LS and S), low eccentric x_2 is turned into x_1 , unstable sequence x_3 of S-orbits is turned into unstable sequence x_3' of L-orbits (panel LS). Changing of the sign of b results only in the horizontal shift of all portraits by $\pi/2$.

¹ The first letter in the panel labelling shows the orientation of the closed stable orbit with smaller eccentricity.

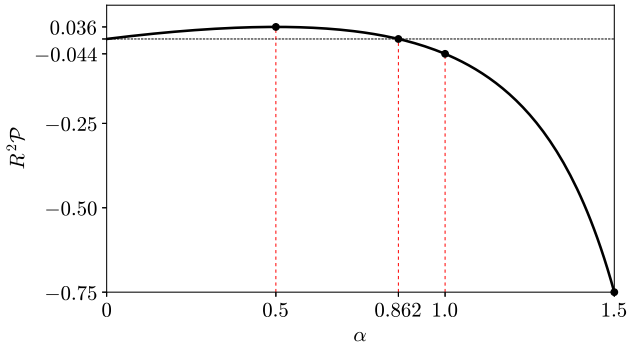


Figure 3. Dependence of $R^2\mathcal{P}$ versus α in the power-law potentials.

3 EXAMPLES

3.1 Power-law potentials

This type of potentials include motion in Keplerian and harmonic potentials, and the Mestel disc with a flat rotation curve. Let's assume the angular speed in the form $\Omega(R) = \Theta R^{-\alpha}$. It is easy to show that

$$\mathcal{Q} = \Theta R^{-\alpha} \cdot \left(1 - \sqrt{1 - \alpha/2}\right) - \Omega_p, \quad (3.1)$$

and

$$\mathcal{P} = \frac{\alpha}{2R^2} \left[\left(\frac{8}{2-\alpha}\right)^{1/2} - \frac{3}{4} - \frac{\alpha}{6} - \frac{2}{2-\alpha} \right]. \quad (3.2)$$

Curve $R^2\mathcal{P}$ versus α is given in Fig. 3. It turns out that in power-law potentials, all nearly circular orbits could be either ‘normal’ if $\alpha > 0.862$, or ‘abnormal’ if $\alpha < 0.862$. Note that this boundary is close to $\alpha_{\text{BW}} = 7/8$ of the Bahcall & Wolf (1976) density profile ($\propto r^{-7/4}$).

The ‘normal’ orbits naturally trap along the short axis of the potential inside ILRs $\mathcal{Q} > 0$ (portrait S), but they can be trapped along the long axis outside ILRs if $b < b_{\text{crit}}$ (portrait LS). On the opposite, the ‘abnormal’ orbits naturally trap along the long axis of the potential beyond the resonance (L) but can be trapped along the short axis if b is sufficiently small (SL).

3.2 The isochrone potential

Consider the isochrone potential

$$\Phi(r) = -\frac{GM}{a + (a^2 + r^2)^{1/2}}, \quad (3.3)$$

for which the Jacobi integral reads:

$$H_0 = -2G^2M^2t^{-2} - \Omega_p L \quad (3.4)$$

where $t = 2J_f + s$, $s = (L^2 + 4GMa)^{1/2}$. The LB-derivative of the precession rate can be obtained explicitly for any orbit (see also Lynden-Bell 1979):

$$\frac{\partial \Omega_{\text{pr}}(L, J_f)}{\partial L} = \frac{4G^2M^2}{s^3t^4} (4GMat - 3L^2s). \quad (3.5)$$

In the limit of circular orbits (small I), one can use (2.13) or put $t = L + s$ in eq. (3.5).

Fig. 4 a shows angular speed Ω , $\Omega_i \equiv \Omega - \varkappa/2$, and two bar pattern speeds above and below the maximum of Ω_i . The

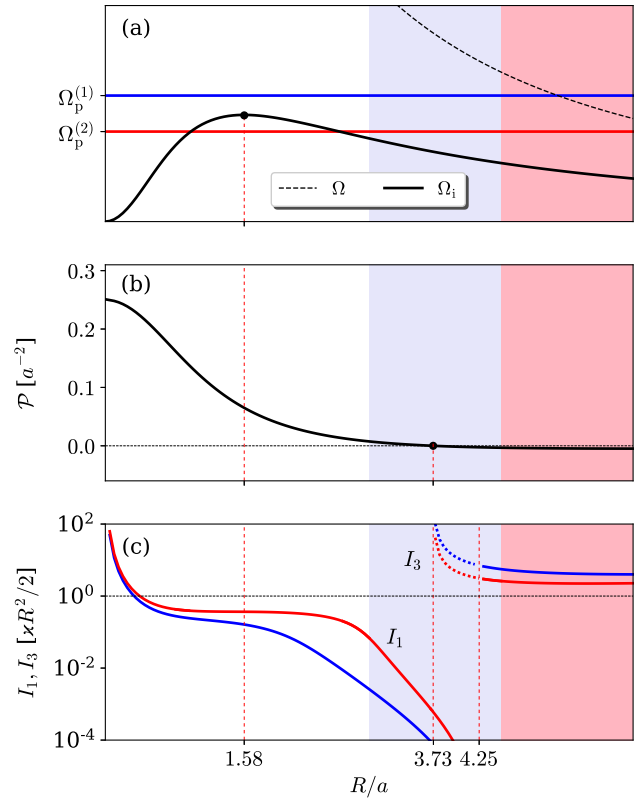


Figure 4. Isochrone potential: (a) angular speed Ω , $\Omega_i \equiv \Omega - \varkappa/2$, and two pattern speeds $\Omega_p^{(1)}$ and $\Omega_p^{(2)}$; (b) LB-derivative (2.13); (c) stationary points I_1, I_3 for the pattern speeds in (a) in units of $\varkappa R^2/2$ for model bar potential (3.6), $\varepsilon = 0.1$ (same colour coding). Solid/dotted lines in (c) show sequences x_1/x_2 . Blue/pink shades show where the slowness assumption breaks down for $\Omega_p^{(1)}/\Omega_p^{(2)}$. Ticks at 1.58, 3.73 and 4.25 mark maximum of Ω_i and zeros of \mathcal{P} and b , correspondingly.

slowness assumption is valid in the unshaded area for the larger pattern speed and breaks down further out. Similarly, for the smaller pattern speed, it breaks down in the pink area. Intersections of the pattern speed horizontal lines with angular speed $\Omega(r)$ give positions of corotation resonances, where the assumption is invalid.

The middle panel presents the LB-derivative \mathcal{P} in units a^{-2} . It is positive inside $R = 3.73a$, and negative but vanishingly small outside this circle. This behaviour is natural and expected because of the damping factor R^{-2} at large distances, see eq. (3.2).

Let's assume a model bar potential in the form:

$$A(r) = -\varepsilon \frac{GM}{2a^2} r e^{-r/a}. \quad (3.6)$$

From (2.14) we infer that sign of b is determined by sign of expression $(1 - R/a + 4\Omega/\varkappa)$, which switches from positive to negative at $R = 4.25a$.

Panel (c) of Fig. 4 illustrates the characteristic curves of sequences x_1 and x_2 for a matured bar only, $\varepsilon = 0.1$ (the bar amplitude is still small compared to the axisymmetric background). The stationary points I_1 and I_3 are obtained from (2.17) and (2.18). Curves I_1 are similar for these pattern speeds: despite two ILRs present for the red curve, the sequence x_1 corresponding to I_1 does not change to x_2 , as it

happens in the theory of weak bars. The family of S-orbits does not appear for $Q > 0$, because b exceeds the critical value b_{crit} .

Solutions I_3 formally exist beyond $R = 3.73$ but they obviously violate the epicyclic approximation. Note that it also breaks down for I_1 in the very centre, because $\varkappa R^2/2$ vanishes there.

3.3 The Milky Way model

The model we use here was elaborated in detail in our previous paper (Polyachenko et al. 2016). It consists of three components: thin exponential disc, Sércic bulge and NFW halo. The disc is characterised by the radial scale $R_d = 2.9$ kpc, vertical scale $z_d = 300$ pc and mass $M_d = 4.2 \cdot 10^{10} M_\odot$ (solar mass). The bulge has a weak cuspy density profile in the centre $\rho_b \propto r^{-1/2}$, and mass $M_b \approx 10^{10} M_\odot$. The total circular velocity is bulge-dominated at radii $R \lesssim 2.5$ kpc, and halo-dominated at $R > 9$ kpc. At radius $R = 6$ kpc, where the disc contribution peaks, the force from the halo is about 2/3 of the force from the disc in the galactic plane.

N-body simulations show bar instability producing a bar rotating with pattern speed $\Omega_p = 55$ km/s/kpc. A bar amplitude grows exponentially in time with a small growth rate $\gamma \sim 0.07 \Omega_p$ and saturates at the level 10...20 per cent of the axisymmetric background. After that, the amplitude stays nearly constant, but the bar pattern speed gradually decreases.

It is well known that ILR damps spiral waves (Mark 1974)². Through this effect, the bar formation is suspended in flat disc galaxies. However, the bar can still be formed if ILR radius is comparable with or smaller than the disc vertical scale. Moreover, the bar pattern speed and the growth rate can be reproduced well from the linear perturbation theory for flat discs, if one uses an angular speed $\bar{\Omega}$ averaged over vertical axis z , instead of in-plane Ω calculated from the total axisymmetric potential (Polyachenko et al. 2016).

Fig. 5 a shows the in-plane Ω and Ω_i , z -averaged $\bar{\Omega}_i$, and the initial bar pattern speed Ω_p . A vertical dashed line at $R = 0.55$ kpc marks the maximum of $\bar{\Omega}_i$. Curve $\mathcal{P}(R)$ on panel (b) is calculated using $\bar{\Omega}$. Similar to Fig. 4 b, it is positive in the centre, and is slightly negative beyond $R = 1.73$ kpc.

Panel (c) presents characteristic curves of sequences x_1 and x_2 for $\bar{\Omega}_i$ and the maximum bar amplitude b obtained from N-body snapshots (in particular, $T = 1.3$ Gyr). These curves are qualitatively similar to those shown on Fig. 4 c. In particular, the central part is populated with x_1 orbits only. The sequence x_2 formally obtained beyond 1.73 kpc consists of too eccentric orbits to be represented in the galactic disc (red dots show typical radial actions populated in the disc). Notably, the curves of sequences for the in-plane Ω come almost the same as for $\bar{\Omega}_i$ (dashed line for I_1 , not shown for I_3).

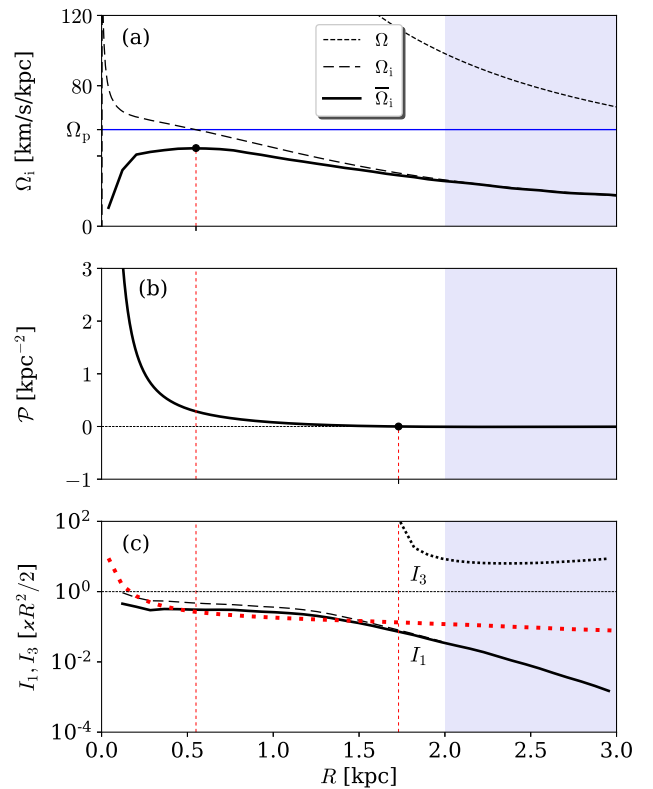


Figure 5. Same as Fig. 4 for the Milky Way model: (a) Ω_i (long dashes) now marks the in-plane quantity, while $\bar{\Omega}_i$ (solid) marks the quantity averaged over the vertical axis (see text); pattern speed of the bar Ω_p , as obtained in N-body simulations (Polyachenko et al. 2016); (c) stationary points I_1 , I_3 for the maximum bar potential (the line type coding corresponds to panel (a) and Fig. 4 c). Red dots show $\sigma^2/\varkappa^2 R^2$ – typical normalised radial actions populated in the disc (σ is the radial velocity dispersion). Ticks at 0.55 and 1.73 mark maximum of $\bar{\Omega}_i$ and zero of \mathcal{P} .

4 DISCUSSION AND SUMMARY

Using the standard technique of finding stationary points of the Hamiltonian, we show that orientation of orbits is governed by the signs of the precession rate \mathcal{Q} , of the LB-derivative³ of the precession rate \mathcal{P} , and of the orbital responsiveness to the bar potential b . This is in accordance with our previous works based on the matrix methods of the linear perturbation theory that show the importance of the sign of the precession rate for radial-orbit (Polyachenko et al. 2010a, 2015; Polyachenko & Shukhman 2015, 2017) and loss cone instabilities (Polyachenko et al. 2007, 2008, 2010b).

These new results extend the theory of bar formation by Lynden-Bell (1979) that classifies all disc orbits using only one of these three parameters – the sign of \mathcal{P} . A majority of orbits consist of so-called ‘normal’ orbits characterised by the negative sign of \mathcal{P} . It tends to align in the direction perpendicular to the bar. The smaller fraction of orbits

² In the purely linear theory. The nonlinear effects near ILR can deactivate damping (Polyachenko & Shukhman 2019).

³ The derivative over angular momentum at constant adiabatic invariant J_f .

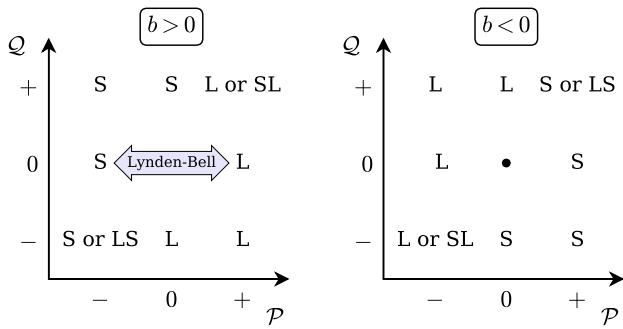


Figure 6. The phase portraits for $b > 0$ (left) and $b < 0$ (right). Double arrow marks two cases suggested by Lynden-Bell (1979).

populating the central part of the disc called ‘abnormal’, for which $\mathcal{P} > 0$, aligns with the bar thereby reinforcing it.

The progress of the current work is two-fold. First, the inclusion of the second parameter Q leads to a variety of combinations for orbits to align with the bar. Fig. 6 condenses the phase portraits types for any possible combination. The portraits given in Fig. 2 contain the stationary points corresponding to the well-known sequence x_1 of the orbits aligned parallel to the long axis, as well as stable sequence x_2 and unstable sequence x_3 of the orbits aligned parallel to the short axis of the potential perturbation.

Second, analysis of the realistic models shows that although formally \mathcal{P} is negative outside the central region, it is small in the absolute value. This discriminates the role of so-called ‘normal’ orbits to destroy the bar. Indeed, the presence of Q -term allows to put $\mathcal{P} = 0$ in this region, thus the portraits for $\mathcal{P} < 0$ can be essentially ignored.

Section 3.3 presents a simple Milky Way model with a weak cusp in the centre $\rho \propto r^{-1/2}$ and nearly flat rotation curve outside $R = 1.5 \dots 2$ kpc circle (see Fig. 7 of Polyachenko et al. 2016). In the inner disc, the positive sign of \mathcal{P} plays a major role in determining the orientation of orbits along the potential well. However, if $Q > 0$, our theory predicts a family of short-axis orbits (S-orbits) for small b (portrait SL). This presumably explains the well-known phenomenon (e.g., Combes & Elmegreen 1993) that bars in N-body simulations have pattern speeds larger than the maximum of Ω_i (i.e. $Q < 0$) because S-orbits in case of $Q > 0$ immediately destroy low amplitude bar-like perturbations. Only perturbations with $Q < 0$ can be reinforced by trapping the orbits along the potential well. Remarkably, the matured bar can sustain the pattern speed decrease below the maximum of Ω_i , because for large b only L-orbits are possible.

In the outer disc beyond point $\mathcal{P} = 0$, orbits continue to add to the bar unless the bar pattern speed is too low so that the orbits find themselves between two ILR’s, i.e. $Q > 0$.

In the theory of weak bars (Sanders & Huntley 1976; Sellwood & Wilkinson 1993), the epicyclic approximation (2.8) is used to derive orientations of nearly circular orbits. Below we follow sect. 3.3.3 of BT to compare their closed loop orbits with ours. Their ‘epicyclic radius’ is

$$C_2 = -\frac{A}{R\Delta} \left(\frac{R}{A} \frac{dA}{dR} + \frac{2\Omega}{\Omega - \Omega_p} \right), \quad (4.1)$$

where $\Delta = \kappa^2 - 4(\Omega - \Omega_p)^2$. Near the resonance $\kappa \approx 2(\Omega - \Omega_p)$, so Δ can be substituted by $-4Q\kappa$. The corresponding radial action is then

$$I = \frac{\kappa}{2} C_2^2 \approx \frac{\kappa}{2} \frac{A^2}{16R^2 Q^2 \kappa^2} \left(\frac{R}{A} \frac{dA}{dR} + \frac{4\Omega}{\kappa} \right)^2. \quad (4.2)$$

The last expression coincides with our stationary point I_1 for L-orbits obtained from (2.18) outside ILRs, provided $\mathcal{P} = 0$ (see also Goldreich & Tremaine 1981).

The ‘epicyclic radius’ C_2 formally changes its sign at the inner and outer ILRs due to Δ , resulting in appearance of x_2 sequence of orbits perpendicular to the potential well (x_1 - x_2 - x_1 sequence in Fig. 3.20 of BT). From our theory it follows (Fig. 5 c) that orbits’ orientation along the potential well is retained between the resonances for large bar amplitudes (c.f. Fig. 3.18 of BT). Note that in case of the weak bar, the L-orbit family continues smoothly across the resonances, but additional S-orbit family appears around smaller I_1 .

The parameter b becomes negative at radius R_b where the round bracket in (2.14) vanishes. The physical meaning of this radius is the last closed orbit of x_1 sequence, so it can be used as a clearly detectable proxy of the bar length (see also Martinez-Valpuesta et al. 2006). At R_b the LB-derivative is likely to be nearly zero and the precession rate $Q < 0$.

Summarizing the above, two quantities specify the direction of orbit’s trapping with respect to the potential well: the precession rate Q and the LB-derivative of the precession rate \mathcal{P} . Their interplay allows us to explain the features of bar formation observed in N-body simulations and reconcile the Lynden-Bell theory with the theory of weak bars. The third parameter b describing the orbits’ responsiveness to the potential, may alter the orbital alignment, but this may only happen well outside the central region.

ACKNOWLEDGMENTS

This work was supported by the Deutsche Forschungsgemeinschaft (DFG, German Research Foundation) – Project-ID 138713538 – SFB 881 (“The Milky Way System”, subproject A06), by the Volkswagen Foundation under the Trilateral Partnerships grant No. 97778, by RFBR grant 20-52-12009, Foundation for the advancement of theoretical physics and mathematics “Basis” and by Department of Physical Sciences of RAS, subprogram ‘Interstellar and intergalactic media: active and elongated objects’. The work also was partially performed with budgetary funding of Basic Research program II.16 (Ilia Shukhman).

DATA AVAILABILITY

Data underlying this article will be shared on reasonable request to the authors via epolyach@inasan.ru. Data related to the initial conditions may be reproduced via the publicly available software GalactICS.

REFERENCES

Bahcall J. N., Wolf R. A., 1976, ApJ, 209, 214

- Bertin G., 2014, Dynamics of Galaxies. Dynamics of Galaxies. 2nd edn. Cambridge Univ. Press, Cambridge, UK
- Binney J., Tremaine S., 2008, Galactic Dynamics: Second Edition. Princeton University Press
- Combes F., Elmegreen B. G., 1993, A&A, 271, 391
- Contopoulos G., 1975, ApJ, 201, 566
- Goldreich P., Tremaine S., 1981, ApJ, 243, 1062
- Lynden-Bell D., 1979, MNRAS, 187, 101
- Mark J. W.-K., 1974, ApJ, 193, 539
- Mark J. W. K., 1976, ApJ, 203, 81
- Martinez-Valpuesta I., Shlosman I., Heller C., 2006, ApJ, 637, 214
- Merritt D., 1985, AJ, 90, 1027
- Palmer P. L., 1994, Stability of collisionless stellar systems: mechanisms for the dynamical structure of galaxies. Vol. 185, Kluwer, Dordrecht
- Polyachenko E. V., 2004, MNRAS, 348, 345
- Polyachenko E. V., 2005, MNRAS, 357, 559
- Polyachenko E. V., Berczik P., Just A., 2016, MNRAS, 462, 3727
- Polyachenko E. V., Polyachenko V. L., Shukhman I. G., 2007, MNRAS, 379, 573
- Polyachenko E. V., Polyachenko V. L., Shukhman I. G., 2008, MNRAS, 386, 1966
- Polyachenko E. V., Shukhman I. G., 2015, MNRAS, 451, 601
- Polyachenko E. V., Shukhman I. G., 2017, MNRAS, 470, 2190
- Polyachenko E. V., Shukhman I. G., 2019, MNRAS, 483, 692
- Polyachenko E. V., Shukhman I. G., 2020, Astronomy Letters, 46, 12
- Polyachenko V. L., 1991, Soviet Astronomy Letters, 17, 371
- Polyachenko V. L., Polyachenko E. V., Shukhman I. G., 2010a, Astronomy Letters, 36, 86
- Polyachenko V. L., Polyachenko E. V., Shukhman I. G., 2010b, Astronomy Letters, 36, 175
- Polyachenko V. L., Polyachenko E. V., Shukhman I. G., 2015, Astronomy Letters, 41, 1
- Saha P., 1991, MNRAS, 248, 494
- Sanders R. H., Huntley J. M., 1976, ApJ, 209, 53
- Sellwood J. A., Wilkinson A., 1993, Reports on Progress in Physics, 56, 173
- Shu F. H., 1969, ApJ, 158, 505
- Tremaine S., 2005, ApJ, 625, 143
- Weinberg M. D., 1991, ApJ, 368, 66